The Journal of Chemical Physics ARTICLE scitation.org/journal/jcp

Charge transfer dynamics and interlayer exciton formation in MoS_2/VOPc mixed dimensional heterojunction

Cite as: J. Chem. Phys. 157, 184701 (2022); doi: 10.1063/5.0107791
Submitted: 6 July 2022 • Accepted: 19 October 2022 •
Published Online: 8 November 2022

Madison C. Schwinn,[1,2,3] Shahnawaz Rafiq,[1] Changmin Lee,[1] Matthew P. Bland,[4] Thomas W. Song,[4] Vinod K. Sangwan,[4] Mark C. Hersam,[1,2,4,a)] and Lin X. Chen[1,2,3,a)]

AFFILIATIONS

[1] Department of Chemistry, Northwestern University, Evanston, Illinois 60208, USA
[2] Graduate Program in Applied Physics, Northwestern University, Evanston, Illinois 60201, USA
[3] Chemical Science and Engineering Division, Argonne National Laboratory, Lemont, Illinois 60439, USA
[4] Department of Materials Science and Engineering, Northwestern University, Evanston, Illinois 60208, USA

Note: This paper is part of the JCP Special Topic on Photophysics in Emerging Photovoltaics.
[a)] **Authors to whom correspondence should be addressed:** m-hersam@northwestern.edu and l-chen@northwestern.edu

ABSTRACT

Mixed-dimensional van der Waals heterojunctions involve interfacing materials with different dimensionalities, such as a 2D transition metal dichalcogenide and a 0D organic semiconductor. These heterojunctions have shown unique interfacial properties not found in either individual component. Here, we use femtosecond transient absorption to reveal photoinduced charge transfer and interlayer exciton formation in a mixed-dimensional type-II heterojunction between monolayer MoS_2 and vanadyl phthalocyanine (VOPc). Selective excitation of the MoS_2 exciton leads to hole transfer from the MoS_2 valence band to VOPc highest occupied molecular orbit in ~710 fs. On the contrary, selective photoexcitation of the VOPc layer leads to instantaneous electron transfer from its excited state to the conduction band of MoS_2 in less than 100 fs. This light-initiated ultrafast separation of electrons and holes across the heterojunction interface leads to the formation of an interlayer exciton. These interlayer excitons formed across the interface lead to longer-lived charge-separated states of up to 2.5 ns, longer than in each individual layer of this heterojunction. Thus, the longer charge-separated state along with ultrafast charge transfer times provide promising results for photovoltaic and optoelectronic device applications.

I. INTRODUCTION

Mixed-dimensional heterojunctions (MDHJs) are an emerging class of materials that involve the combination of materials with different dimensionalities through non-bonding van der Waals (vdW) forces. The constituent nanomaterials can be zero-dimensional (0D), such as fullerenes, organic molecules, and quantum dots;[1,2] one-dimensional (1D), such as nanotubes, nanowires, and polymers;[3,4] and two-dimensional (2D), such as graphene, transition-metal dichalcogenides, and hexagonal boron nitride.[5–8] These nanomaterials can be integrated between themselves or three-dimensional (3D) conventional semiconductors to realize unprecedented functionalities and applications. MDHJs involving van der Waals materials can bypass limitations of conventional heterostructures, where direct chemical bonding or lattice matching is required.[9,10] Instead, vdW forces can easily merge the materials and retain their intrinsic properties that are useful to optoelectronic devices, such as high optical absorption, high fluorescence quantum yields, and higher carrier mobility.[11] MDHJ between 2D and 0D materials is particularly interesting for functional photodetectors,[12] photocatalysts,[13,14] phototransistors,[15,16] and ultracompact photovoltaics.[17]

The combination of semiconducting 2D transition metal dichalcogenides (TMDs) with 0D organic molecules has received significant traction in the electronic materials and devices community.[13,15,18–23] On their own, semiconducting monolayers

such as MoS_2 and WS_2 have a direct bandgap[24] and high carrier mobility,[12] but they are prone to defects and interfacial interactions that lead to lower fluorescence quantum yields.[25,26] Organic semiconductors, on the other hand, have high optical absorption and high fluorescence quantum yields,[11] but they suffer from lower carrier mobilities.[27] While each of these types of materials has been independently used to create photovoltaic and optoelectronic devices,[28] combining them could potentially passivate defects, increase carrier mobility, and improve radiative recombination yields.[29,30] The interaction of a 2D semiconductor and organic molecule can result in different excitonic interactions than in 2D/2D and all-organic heterostructures. The organic layer has more tightly bound Frenkel excitons, while excitons in the 2D layer are closer to delocalized Mott–Wannier excitons.[31] As a result, the interlayer excitons that form at the interface may have differing degrees of localization or delocalization.[32] These interlayer excitons have longer charge recombination times,[19,33,34] and when used in devices, they have had higher internal quantum efficiency in processes that rely on the dissociation of the delocalized excitons into free carriers at the interface.[35]

Free base and metalated phthalocyanine (MPc) such as H_2Pc,[36,37] ZnPc,[33,38] and CuPc[37] have been integrated with 2D monolayer semiconductors such as MoS_2.[39] The interlayer charge transfer and exciton dynamics are particularly interesting in these heterojunctions because of the complexity of their electronic interfaces. Most of these MDHJs have a type-II band alignment with monolayer MoS_2; hence, upon photoexcitation, the electrons can transfer from the lowest unoccupied molecular orbit (LUMO) of MPc to the conduction band minima (CBM) of MoS_2 and, likewise, holes can transfer from valence band maxima (VBM) of MoS_2 to highest occupied molecular orbit (HOMO) of MPc.[11] Either of these processes can form interlayer excitons, also known as charge transfer excitons, across the heterointerface, which can lead to long exciton and charged carrier lifetimes. These MDHJs have shown to exhibit over ten times longer lived charge-separated states[19,33,34] than in 2D/2D heterostructures,[37,40] which are favorable for photovoltaics and photodetection applications.[23]

Vanadyl phthalocyanine (VOPc) from the class of metal phthalocyanines is a large semiconducting macrocyclic molecule, where vanadyl (VO^{2+}) is coordinated with the four nitrogen atoms of the Pc macrocycle.[41,42] VOPc has high third-order nonlinear optical susceptibilities,[43] has a molecular plane stacked parallel to the bulk MoS_2 surface,[44] and has shown efficient charge transport along the π-stacking direction.[45] Previous work on this heterojunction reported the formation of an emissive interlayer exciton, but more detailed work on the charge transfer dynamics is essential for understanding the formation of interlayer excitons.[22] In this work, we use femtosecond transient absorption (fs-TA) to study the ultrafast carrier dynamics of the MoS_2/VOPc heterojunction, with a focus on early time charge transfer and exciton dynamics. We excite the heterojunction at MoS_2 and VOPc selective pump wavelengths and use spectral evolution, kinetic trace analysis, and global analysis to determine a 710 fs hole transfer and sub-100 fs electron transfer across the interface. We provide evidence for the formation of interlayer excitons by the selective excitation of the two components of this type-II heterojunction, where the formation of an interlayer exciton is limited by carrier transfer rates between the MoS_2 and VOPc layers.

II. EXPERIMENTAL

A. Sample preparation

Continuous films of monolayer MoS_2 were grown on sapphire substrates using solid precursor chemical vapor deposition (CVD) by modifying the procedure previously described.[46] The detailed growth process is outlined in Sec. S1 of the supplementary material. The thickness and quality of the monolayer MoS_2 were confirmed by photoluminescence spectroscopy and Raman microscopy [Fig. 1(b) and Figs. S1–S4 of the supplementary material].

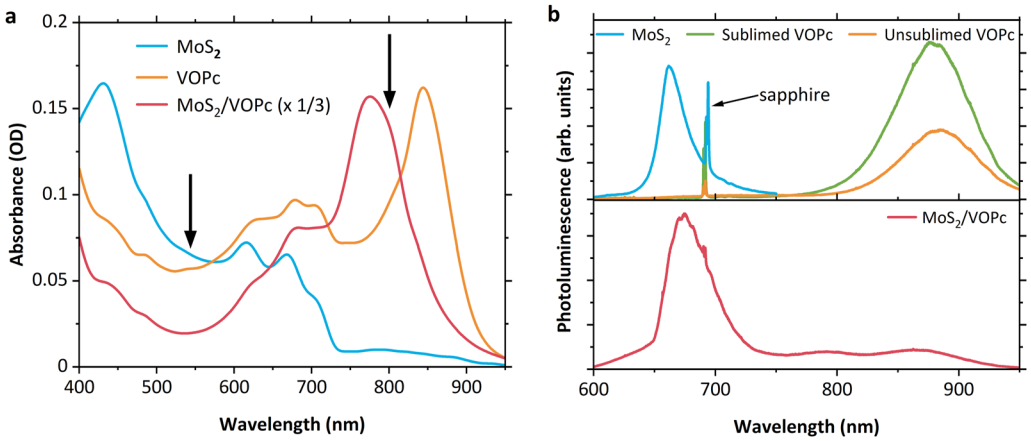

FIG. 1. (a) Ground state absorption spectra of monolayer MoS_2 (blue), 5 nm VOPc (orange), and MoS_2/VOPc MDHJ (red), all on sapphire. Arrows indicate preferential excitation wavelengths for MoS_2 at 540 nm and VOPc at 800 nm, respectively. Absorbance of MoS_2/VOPc heterojunction has been downscaled to compare amplitudes to bare MoS_2 and VOPc samples. (b) Photoluminescence spectra (Excitation = 532 nm, NA = 0.95) of bare MoS_2, sublimed VOPc, unsublimed VOPc (top panel), and MoS_2/VOPc heterojunction (lower panel), all on the sapphire substrate. The sharp peaks at 693 nm are due to the sapphire substrate.

Vanadyl phthalocyanine (VOPc) powder of purity (>90%) was purchased from Sigma-Aldrich. A film of VOPc (thickness = 5 nm) was grown on MoS_2-coated sapphire substrates by using a thermal evaporator that is housed inside an inert N_2 glove box (rate = 0.1 Å/s). We further confirmed that Raman spectra of grown VOPc film and VOPc powder are consistent with previously reported spectra of VOPc crystals (Fig. S2 of the supplementary material).[47] Purification of VOPc was performed via gas sublimation. Commercial VOPc powder was heated in a tube furnace at 400 °C and 70 mTorr. A temperature gradient of 100 °C is maintained to allow the VOPc to recrystallize further downstream.[48] We compared purified VOPc and commercial VOPc via photoluminescence and Raman and show that the spectra of the VOPc films from sublimed and unsublimed (>90%) materials showed strong agreement. Residual contaminants are not expected to affect the crystal structure and conclusions of this study. Since transient absorption spectroscopy required high optical transparency of 5-nm-thick VOPc in the VOPc-MoS_2 heterojunction, we also confirm the Raman spectra of stand-alone thicker (30 nm) VOPc films and 5-nm-thick VOPc in the heterojunction (Fig. S4 of the supplementary material). Despite the weak Raman signal in the 5-nm-thick film, we can identity 90% of all the peaks (total 19 peaks), suggesting that the crystal structure of VOPc does not change significantly in the heterojunction. The surface morphology of VOPc film was characterized by atomic force microscopy (Fig. S5 of the supplementary material). The thickness of VOPc film (≈5 nm) was confirmed by atomic force microscopy (AFM) topography imaging across the step height of the VOPc film grown on the bare sapphire substrate (Fig. S6 of the supplementary material).

B. Femtosecond transient absorption (fs-TA)

Laser pulses for fs-TA were generated from the Ti: sapphire oscillator (Mira, Coherent, Inc.) and the regenerative amplifier (RegA Model 9000, Coherent, Inc.). The generated fundamental pulses were at 800 nm at a repetition rate of 250 kHz. The pulse energy was 6 μJ, and the pulse duration was 60 fs. A majority of the beam was used to generate a 540 nm beam through an optical parametric amplifier (OPA model 9400, Coherent, Inc.) with 160 nJ pulse energy and 40 fs pulse width, which was used as the pump excitation pulse. Thus, 800 nm pump pulses were made without the OPA. The remaining 800 nm pulses were focused into a sapphire crystal to produce white light probe pulses. The delay stage was put at the pump line to generate optical delay between the pump and the probe. The pump and the probe beam polarizations were parallel. After passing through the monochromator (Acton SP2300, Princeton Instruments), the probe beam was dispersed and sent to the charge-coupled device (CCD, PIXIS100, Princeton Instruments) detector. The chirp in the TA signal generated from the materials was post-corrected via rising edge fit applying the quadratic relation $t = a\lambda^2 + b\lambda + c$. Each sample was measured at several locations and then averaged.

Transient absorption data were background subtracted and chirp corrected with a written Matlab R2021b code, and plots were generated with OriginLab 2021 pro. Single kinetic traces were fit with a multi-exponential decay function convoluted with a Gaussian instrument response function (IRF). Global analysis was performed with open-source software Glotaran.[49]

C. UV–vis, Raman, and photoluminescence spectroscopy

Absorption spectra were measured using Shimadzu UV–vis NIR spectrophotometer (UV-3600). Several positions on each sample were measured, and the spectra were averaged to minimize the heterogeneity of the film samples. Raman and photoluminescence spectra were obtained in a Horiba LabRAM HR Evolution setup by using an excitation wavelength of 532 nm. For Raman, the scattered light was collected by a 100× objective (NA = 0.95) and dispersed with a grating of 2400 groove/mm before analyzing in a CCD camera. For photoluminescence, the emitted light was collected by the same 100× objective and dispersed with a grating of 600 groove/mm.

III. RESULTS AND DISCUSSION

A. Absorption and photoluminescence spectra

Figure 1(a) shows the ground state film absorption spectra of MoS_2, VOPc, and the MoS_2/VOPc heterojunction. In bare MoS_2 (blue line), two excitonic absorption peaks arise from spin orbit splitting in the valence band and are labeled the A and B excitons, located at 668 and 616 nm, respectively.[50] VOPc has a broad 600–750 nm Q-band region and a sharper 850 nm peak. The absorption of VOPc can vary based on phase and growth conditions; however, the absorbance of our VOPc on sapphire has the characteristics of the polycrystalline phase II structure.[51,52] The MoS_2/VOPc heterojunction (red line) shows contributions from both materials, such as the MoS_2 A and B excitons and VOPc 850 nm peak. Compared to the VOPc on sapphire, the VOPc on MoS_2 in the heterojunction has a blue-shifted Q-band absorption peak at 775 nm. A similar peak shift has been reported previously in stand-alone VOPc films grown on sapphire and was ascribed to the change from crystalline to amorphous forms.[52] Thus, we suggest that the absorption peak shift in the heterojunction is due to a change from polycrystalline VOPc on sapphire to amorphous VOPc on MoS_2. Similar morphology variation has been observed in pentacene grown on MoS_2, SiO_2, and hBN, where atomically flat and inert hBN substrates enabled larger crystalline domains.[53] Thus, the atomically flat and inert sapphire substrate is expected to be conducive for larger crystallinity in VOPc domains. This morphology change may also be responsible for the overall absorption intensity increase seen in the heterojunction relative to the bare VOPc and MoS_2 samples. The apparent red-shifted MoS_2 bands are likely due to interfacial electronic interactions between the very thin layers of MoS_2 and VOPc.

Photoluminescence spectra (PL) were compared between bare (control) monolayer MoS_2, bare VOPc (sublimed and unsublimed), and the MoS_2/VOPc heterojunction in Fig. 1(b). Bare monolayer MoS_2 (top panel, blue) shows a strong peak at 660 nm corresponding to the A exciton.[17,31,36,40,54–57] Both unsublimed (orange) and sublimed (green) VOPc show a broad peak at 880 nm (top panel), consistent with previous literature.[22,51] We note three main observations from the PL spectra. First, sublimed and unsublimed VOPc show qualitatively similar spectra. Second, the PL of the heterojunction (lower panel, red) has a red-shifted A exciton peak at 674 nm and blue-shifted VOPc peak at 865 nm. The shift in peaks in the heterojunction sample compared to stand-alone samples is expected

due a reduction in the bandgap of MoS_2 from decreased density of free carriers in the depletion region.[17] Third, we observe a new peak in the heterojunction at 790 nm, which is not associated with either VOPc or MoS_2 and can be attributed to the formation of an interlayer exciton.[17,22,32,35]

B. Transient absorption measurements

To investigate the carrier dynamics in the MoS_2/VOPc heterojunction, we use a narrowband 540 nm laser pulse to preferentially excite the MoS_2 layer and subsequently probe the carrier dynamics with a white light spectrum as a function of time. We also use an 800 nm pump pulse that excites a mix of VOPc localized transition as well as the new transition that appears in the spectral region overlapping with the VOPc absorption. These two excitations are shown as arrows in Fig. 1(a). To estimate a relationship between the power pump fluence and absorbance in the samples, power dependent studies were performed at different fluences for the MoS_2 and VOPc samples. We find that the transient absorbance signal varies linearly as a function of the pump fluence indicating that the carrier dynamics reported in this study are in the linear regime (Fig. S7 of the supplementary material). The carrier dynamics reported below were obtained with a 540 nm pump pulse having a pulse energy of 24 nJ and an energy fluence of 0.3 mJ/cm^2, giving an injected carrier density of 8.5×10^{20} cm^{-3}. The pulse energy for the 800 nm pump pulse was 400 nJ with an energy fluence of 5 mJ/cm^2, giving an injected carrier density of 3×10^{21} cm^{-3}.

The TA measurements reported here were measured with parallel polarization of the pump and probe beams. To ensure that no anisotropy is detected in these solid samples, transient absorption spectra were also measured at perpendicular and magic angle polarizations. We found no difference in the kinetics at each polarization; hence, we conclude that there's no detectable anisotropy and the parallel polarization scheme is adequate for our samples.

1. 540 nm excitation of the MoS_2/VOPc heterojunction

Figure 2(a) shows a series of representative transient absorption spectra of the MoS_2/VOPc heterojunction at 540 nm pump excitation at delay times between 250 fs and 1 ns. These spectra are characterized by negative ground state bleach (GSB) from the A and B excitons of MoS_2 at 621 and 672 nm, respectively, along with excited state absorptions (ESAs) on both sides of these bleach features. A similar plot of transient absorption spectra of the bare MoS_2 layer is shown in Fig. 2(b). Here, MoS_2 shows a characteristic transient absorption spectrum with negative bleach signals corresponding to the excitonic transition for the A (616 nm) and B (662 nm) excitons. It also has positive signals corresponding to the ESA from the split structure of the conduction band.[56,58–60] The slight shift in the band position of these MoS_2 excitonic features from that of the steady state absorption is due to bandgap renormalization from repulsive Coulomb interaction in the photoexcited MoS_2 that causes the bandgap to shrink.[61,62] Conversely to the MoS_2 and heterojunction signal, the signal given by exciting the neat VOPc at 540 nm is nearly negligible at 250 fs probe delay [Fig. 2(c), orange line], which is likely due to the relative low extinction coefficient in the spectral valley between the Soret and Q-bands. The non-zero absorbance for VOPc may be due a baseline scatter in the ground state film absorption spectrum [Fig. 1(a)].

For comparative analysis of the control samples and the heterojunction at 540 nm excitation, Fig. 2(c) shows their corresponding spectra at a delay time of 250 fs. At this excitation, the heterojunction shares many of the same features as MoS_2 such as an ESA in the spectral region <600 nm and exciton related GSBs. However, there is a distinct negative signal above 730 nm region in the heterojunction that is not present in the bare MoS_2 layer. This signal is in the same spectral region as the Q-band of the VOPc layer [Fig. 1(a), orange line] and, therefore, must originate from the interaction of MoS_2 with the VOPc layer after photoexciting MoS_2. Considering that the TA signal of the neat VOPc film is essentially negligible throughout the entire probe spectral range [Fig. 2(c)], we believe that the GSB

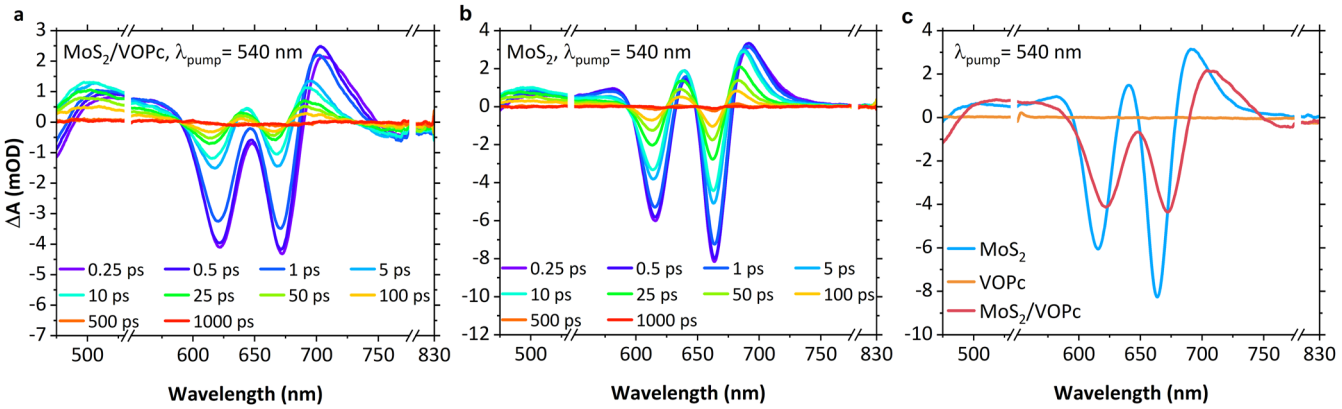

FIG. 2. (a) MoS_2/VOPc heterojunction excited at 540 nm at various delay times. (b) MoS_2 control sample excited at 540 nm at various delay times. (c) MoS_2 (blue), VOPc (orange), and MoS_2/VOPc heterojunction (red) excited at 540 nm at 0.25 ps. The probe region from 530 to 570 nm is not shown due to pump-induced scatter. Similarly, the region from 780 to 810 nm is not shown due to an 800 nm scatter produced by the fundamental probe pulse's interaction with the crystal. Scale is in milli-optical density (mOD).

signal above 730 nm is the consequence of photoexcitation of MoS_2 in the heterojunction film.

Multi-exponential decay fitting was performed for kinetic traces at single probe wavelengths of bare MoS_2 and the heterojunction. For bare MoS_2 pumped at 540 nm and probed at the A exciton (662 nm), the following four time-components (and their fractional amplitudes) provided the best fit to the kinetic trace: $\tau_1 = 1.1 \pm 0.1$ ps (30%), $\tau_2 = 16 \pm 2$ ps (46%), $\tau_3 = 90 \pm 5$ ps (19%), and $\tau_4 = 580 \pm 20$ ps (5%). Similarly, the heterojunction at the A exciton probe wavelength (670 nm) has $\tau_1 = 1.7 \pm 0.2$ ps (63%), $\tau_2 = 10 \pm 1$ ps (25%), $\tau_3 = 140 \pm 7$ ps (8%), and $\tau_4 = 1500 \pm 200$ ps (3%) (Fig. 3). The shortest time constants τ_1 are nearly equal between neat MoS_2 and the heterojunction, but the latter has nearly twice of the relative weight (30% vs 63%). The second component of the heterojunction begins to decay faster than in MoS_2. A faster decay of this excitonic bleach with the addition of VOPc is also seen in the WS_2/tetracene heterojunction and was proposed to be due to the hole transfer process in the heterojunction.[35] We propose that the fast decay of the heterojunction signal as compared to the bare MoS_2 is due to the additional hole transfer pathways that open up upon interfacing MoS_2 with VOPc.

Given the multiple processes expected to occur in MDHJs, single kinetic traces do not always provide a global picture of the complex dynamics undergoing in the photoexcited systems. Instead, a global analysis of the transient absorption data, through decay associated spectra (DAS), provides an interpretation of the various excited state processes through global time constants. In this respect, we applied the singular value decomposition procedure to model the transient absorption data (see Sec. II). The global analysis protocol outputs Decay Associated Spectra (DAS), which are the pre-exponential amplitude of the global time constants at all probe wavelengths. The peaks in DAS reflect loss or gain of carrier population within the specific time and the comparison of DAS report on the various carrier transfer pathways.[63] For example, the positive amplitudes in the GSB region correspond to a rise of the GSB signal, while the negative amplitudes in the same signal correspond to its decay. For an excited state absorption signal, a negative amplitude corresponds to accumulation of the carrier population and a positive amplitude corresponds to the loss of the population.

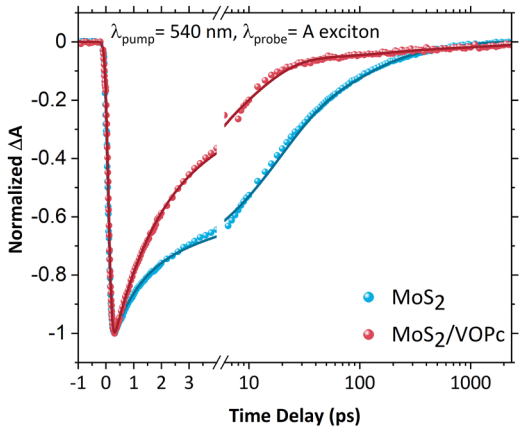

FIG. 3. Normalized kinetic trace and their multiexponential fit of MoS_2 (blue) and MoS_2/VOPc heterojunction (red) excited at 540 nm and probed at the MoS_2 A exciton.

For global analysis of MoS_2/VOPc heterojunction, a minimum of four global time-components were required to accurately fit the transient data. The DAS results for the heterojunction are shown in Fig. 4(a). The first DAS, $\tau_1 = 710 \pm 20$ fs (purple), consists of a growth of the ESA in the spectral region <600 nm and two decaying MoS_2-related bleaching features between 600 and 700 nm. More importantly, there is a growth in a GSB feature above 725 nm [blue and green curves developed from a slight dip in the purple curve in Fig. 3(a)], which is absent in the neat MoS_2 TA spectra [Fig. 2(b)] or DAS (Fig. S8a of the supplementary material). As we suggested above, this GSB feature originates from the interaction between MoS_2 and VOPc. Following that, a growth in this bleach indicates an onset and then increase of the depletion of the ground state of VOPc within 710 fs, which happen as holes are transferred to VOPc.

From reported energy levels of MoS_2[22] and VOPc,[64] the MoS_2/VOPc heterojunction has a type-II band alignment, as visualized in Fig. 4(b). Upon 540 nm photoexcitation of the MoS_2 (with holes in the VB and electrons in the CB), this band alignment allows a hole transfer pathway to form from the VB of MoS_2 to the HOMO of VOPc. This process of hole transfer on a sub-picosecond time scale puts holes in the VOPc layer and electrons in the MoS_2 layer, thereby separating the carries across the interface. In similar type-II MDHJ, this hole transfer from the acceptor to donor material in other 2D–0D heterojunction has been shown to occur on a similar time scale of hundreds of femtoseconds to a few picoseconds.[34,65]

In addition to the sub-picosecond hole transfer, the DAS corresponding to other global time constants are representative of other processes that occur at the interface of MoS_2 and VOPc. The second DAS, $\tau_2 = 3.4 \pm 0.1$ ps (cyan), shows a continuing rise in the ESA signal (<600 nm) and decay of the GSB peaks (A and B excitons of MoS_2). Additionally, the GSB signal in the spectral region >725 nm begins to decay on this time scale. By the third DAS, $\tau_3 = 70 \pm 4$ ps, the ESA is now decaying, and the decay of the GSB regions both decrease in amplitude. The decay of excited state absorption and bleached states are consistent with carrier trapping processes and/or radiative recombination that range from a few to hundreds of picoseconds.[17,33,35,37] In the final DAS, $\tau_4 = 2.5 \pm 0.2$ ns, the amplitudes of all ESA and bleach signals are nearly depleted, representing carriers recombining and returning the system to the ground state within 2.5 ns. Additionally, throughout the DAS spectra, the MoS_2 GSB blue shifts in time. This has been shown as further proof of charge transfer in TMD-based heterojunctions due to electronic screening and bandgap renormalization caused by the transfer of carriers.[20,66]

To summarize, the TA spectral evolution, kinetic trace analysis, and global analysis all point to hole transfer from the MoS_2 to VOPc that occurs within 710 fs. Upon photoexcitation of MoS_2 at 540 nm, holes transfer from the MoS_2 valence band to the VOPc HOMO level. This transfer of holes induces a buildup of charge in the interface of the heterojunction, which bleaches the ground states, as seen in the TA spectra and DAS. This transfer of holes also causes the bandgap of the heterojunction to re-normalize, which results in a blue shift as seen in the spectra.

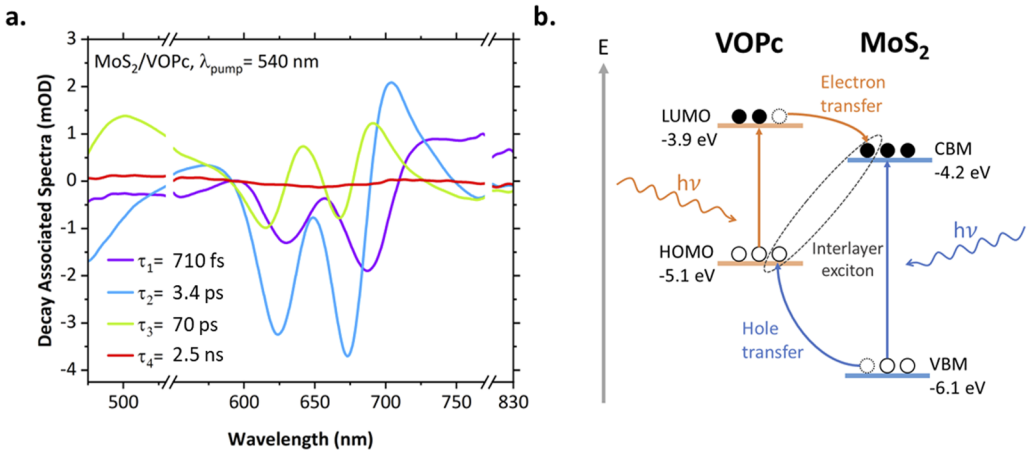

FIG. 4. (a) Decay-associated spectra (DAS) of the heterojunction at 540 nm excitation, obtained with global analysis in Glotaran. (b) Representative diagram of the MoS_2/VOPc type-II heterojunction energy level alignment. Selective excitation of MoS_2 (540 nm) and the following hole transfer are represented in blue, while selective excitation of VOPc (800 nm) and the following electron transfer are represented in orange. Formation of an interlayer exciton is represented by gray dashed line.

2. 800 nm excitation of the MoS_2/VOPc heterojunction

Figure 5(a) presents the transient absorption spectra of MoS_2/VOPc excited at 800 nm at delay times between 250 fs and 1 ns. The transient spectra show a broad ESA in the 450–600 nm region and a strong bleach signal peaked at around 780 nm. In addition, the transient spectra also exhibit bleach features peaked at 620 and 670 nm. Similarly, the transient absorption spectra of bare VOPc at 800 nm excitation are shown in Fig. 5(b). This shows an ESA signature in the 450–600 nm region and a bleach signal peak at ≈820 nm that is associated with its main absorption band as seen in Fig. 1(a).

A comparison of the heterojunction and bare VOPc, shown in Fig. 5(c), indicates that at 800 nm excitation, the heterojunction has two additional bleach bands, as noted above. These bleach signals are not seen in bare VOPc but match with the bleach signals that correspond to the A and B excitons of MoS_2 [Figs. 2(b) and 2(c)]. This is despite MoS_2 having a comparably insignificant signal at an 800 nm excitation wavelength [Fig. 5(c), blue]. Additionally, the GSB in the spectral region >700 nm is broadened and shifted compared to the bare VOPc signal in this region. It appears to match the new band in the ground state absorption spectra at 765 nm. Therefore, the bleach in the heterojunction may represent a mix of the VOPc and this new band GSBs.

To determine how the MoS_2 in the heterojunction pumped at 800 nm changes the dynamics, we compare the kinetic traces of VOPc and the heterojunction probed at 765 nm (Fig. 6). At this wavelength, which probes the GSB seen in both VOPc and the heterojunction, there should be no contribution from MoS_2. Here,

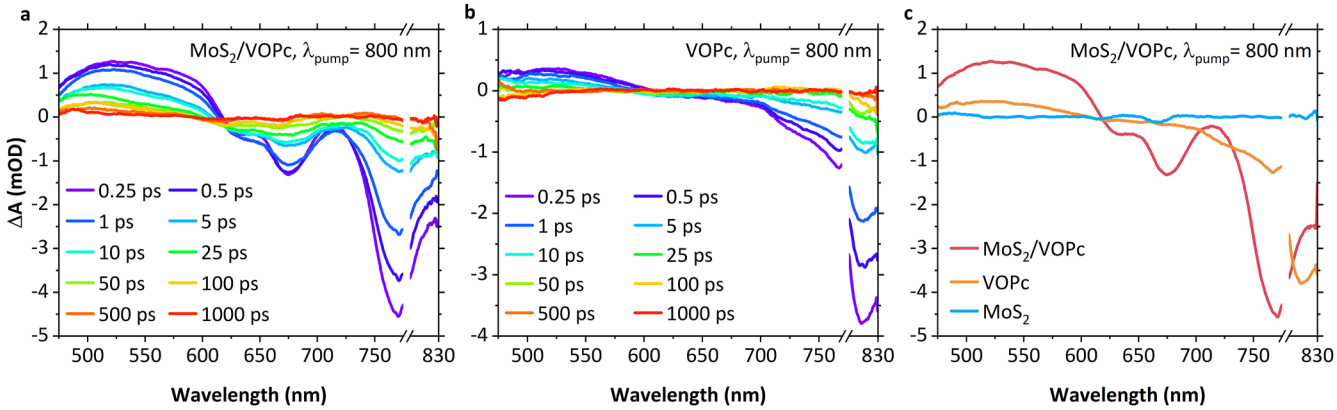

FIG. 5. (a) MoS_2/VOPc heterojunction and (b) VOPc excited at 800 nm at various delay times. (c) Heterojunction (red), VOPc (orange), and MoS_2 (blue) all pumped at 800 nm. The probe range between 790 and 810 nm is not shown due to pump-induced scatter.

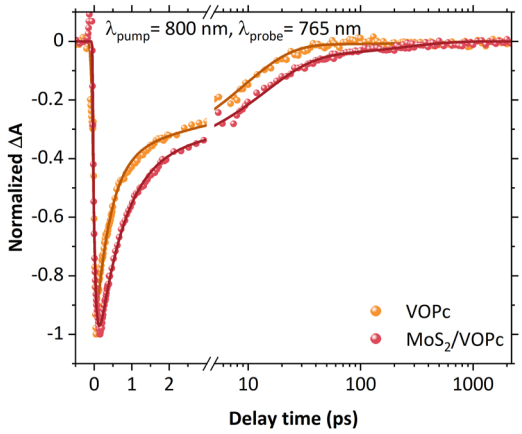

FIG. 6. Linear-log kinetic trace probed at 765 nm GSB in the heterojunction (red) and VOPc (orange), pumped at 800 nm. Points represent raw data, while lines are the fits as listed in Table S1 and the text.

the kinetic trace for VOPc (orange) has time component decays of τ_1 = 500 ± 70 fs (62%), τ_2 = 11 ± 1 ps (36%), and τ_3 = 500 ± 20 ps (2%), and the heterojunction has τ_1 = 60 ± 20 fs (43%) rise and decays at τ_2 = 700 ± 100 fs (38%), τ_3 = 14 ± 2 ps (16%), and τ_4 = 250 ± 15 ps (3%). These kinetic traces and their corresponding time components show that there is a new fast rise-component in the heterojunction not accounted for in bare VOPc, which means the MoS_2 does play a role in the interface dynamics of the heterojunction even when not selectively excited.

Once again, we used global analysis to obtain a fit that elucidates the processes occurring in the entire system, as shown in Fig. 7. Four exponential terms were required to fit our data. In the first DAS, τ_1 = 60 ± 10 fs, the most striking feature is the positive amplitude in the bleach features of the 600–700 nm region, indicating a growth of this bleach. VOPc itself does not have associated bleach features in this region, so this first component is due to MoS_2 and the interlayer effects that stem from that. In previously reported similar

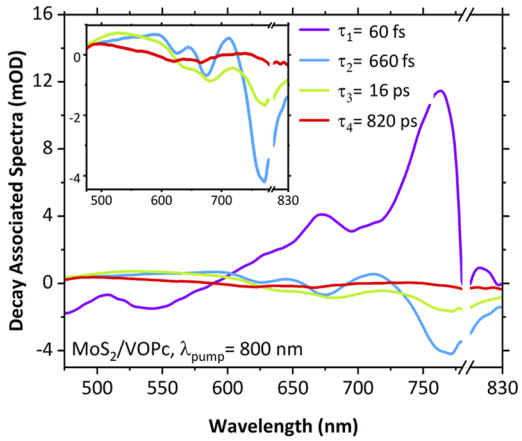

FIG. 7. Decay-associated spectra (DAS) of the heterojunction excited at 800 nm. The break in the spectrum is to exclude pump and probe scatter seen in the 780–800 nm region. Inset: Second, third, and fourth DAS, τ_2–τ_4.

MDHJ, the appearance of the MoS_2 bleaches at wavelengths greater than their bandgap energy has been indicative of an electron transfer that generally happens within the system IRF and has been shown to be as fast as 10 fs.[17,19,33,37] Due to our fit of 60 fs being so close to our IRF, we note that the lifetime of this may be even shorter, so we refer to this value as an approximation. In addition, we also notice a positive signal corresponding to the bleaching of the new 750 nm band in the ground state absorption. This transition is being directly excited by the 800 nm pump, although that positive feature could originate from a fast thermalization process in this state. At such short time scales, there may be a convolution of ultrafast processes such as electron transfer, carrier trapping, and thermalization. Due to this, the growth in bleach may be partly attributed to these other processes that we cannot discern, but we propose that electron transfer is at least partly responsible for this observation.

The inset of Fig. 7 shows the other DAS, excluding the first high-amplitude component. By the second and third DAS, τ_2 = 660 ± 60 fs and τ_3 = 16 ± 2 ps, these GSBs are decaying. As suggested in the 540 nm excitation case, the decaying of the excited and bleach states in heterojunctions is due to radiative recombination and trapping of the electrons.[17,33,35,37] By the final time component of τ_4 = 820 ± 65 ps, the depletion of excited and bleach states is representative of charge recombination processes. The GSBs in the heterojunction are also red-shifted compared to GSBs seen in MoS_2 at 540 nm. It is shifted approximately by the same amount as when the heterojunction is pumped at 540 nm. As seen in PTB7/MoS_2 heterojunction,[19] this is indicative of charge transfer due to conduction band electrons collecting in the acceptor from the excited donor.

The type-II band alignment of this heterojunction means that electron transfer flows energetically downhill from VOPc to MoS_2 upon photoexcitation at the selective VOPc (the electron donor) wavelength. The most promising evidence we see in support of this hypothesis is the appearance of MoS_2 excitonic bleaches, despite it not being directly excited and having an insignificant signal at this pump wavelength. Our first time-component at ~60 fs, as seen in individual kinetic trace fitting (Fig. 6) and DAS (Fig. 7), also supports this hypothesis. There is also an obviously intense growth of the bleach within this timeframe, again indicating a depletion of the ground state upon electron transfer. All this evidence successfully points to a fast electron transfer from the photoexcited VOPc to the valence band of MoS_2 in the MDHJ.

3. Formation of interlayer excitons

The detailed analysis of the transient absorption data at selective excitations confirms the separation of electrons and holes at the MoS_2/VOPc interface. A selective excitation of the MoS_2 layer leads to separation of carriers via hole transfer from the MoS_2 valence band to the VOPc HOMO, while the electrons remain in the conduction band. This hole transfer occurs in 710 fs, as shown in our kinetic traces [Fig. 3(a)] and global analysis [Fig. 4(a)]. In the same manner, a selective excitation of the VOPc layer is followed by an electron transfer from VOPc LUMO directly to the MoS_2 conduction band, leaving behind a hole in the VOPc HOMO. This rapid electron transfer occurs in ~60 fs and separates the electron and hole across the interface. Hence, in exciting either MoS_2 or VOPc, electrons and holes are separated at the interface with electrons in the MoS_2 layer and holes in the VOPc layer. This separation of carriers

across the interface of the heterojunction results in the formation of an interlayer exciton, also known as a charge transfer exciton, as seen in Fig. 4(b).

A direct photoexcitation initially results in the formation of an intralayer exciton in its corresponding layer, which is a bound Frenkel-type in VOPc and Wannier–Mott type in MoS_2.[31] These excitons then dissociate and result in a separation of the carriers across the interface. The formation of the interlayer exciton in itself is limited by the electron or hole transfer times. These generated carriers tend to maintain a strong binding energy of the order of a few hundred meV.[32,35] Thus, they do not dissociate into free carriers and, instead, stay as an exciton. It is due to the formation of this interlayer exciton that we can observe the growth in the bleaching of the excitonic transition that is not directly excited during the selective excitation, as is seen previously in similar systems.[19,24,33,34] Due to the large binding energy of few-hundred millielectron volts, these interlayer excitons tend to undergo radiative or non-radiative recombination, instead of dissociating into free carriers.[18,22,35,66,67] Previous work on MoS_2/VOPc heterojunction suggested that excited carriers relax to mid-gap states, which are emissive in nature and give rise to photoluminescence at lower energies.[22] While we cannot confirm the existence of these mid-gap states in our work, we also observe the emergence of a new PL peak [Fig. 1(b)] at 790 nm along with quenching of MoS_2 and VOPc layers. This possibly indicates the emission of the interlayer excitons in the heterojunction.

In summary, the interface of VOPc and MoS_2 heterojunction facilitates a rapid stepwise carrier transfer process across the heterojunction that leads to the sub-picosecond formation of an interlayer exciton. This formation of the interlayer exciton is limited by the time scale of the hole or electron transfer in the valence or conduction bands, respectively. Typically, these interlayer excitons in other heterojunctions recombine radiatively and lead to photoluminescence, which is what we observe in the MoS_2/VOPc heterojunction.

IV. CONCLUSION

Using femtosecond transient absorption, and related analysis techniques, we have studied the ultrafast charge transfer dynamics and formation of interlayer excitons in the MoS_2/VOPc 2D–0D mixed dimensional heterojunction. Continuous film of polycrystalline monolayer MoS_2 was grown by chemical vapor deposition, while VOPc was deposited by thermal evaporation. We photoexcited the organic and TMD layers of the heterojunction separately to study the role that each material plays on the interfacial physics in the heterojunction. We found that upon using a 540 nm excitation pulse, holes transfer from the photoexcited MoS_2 valence band to the HOMO level in VOPc in 710 fs. Similarly, using an 800 nm pulse, electrons transfer from the photoexcited VOPc LUMO to MoS_2 conduction band in ~60 fs. This electron and hole transfer separates the charges across the interface, leading to the formation of an interlayer exciton.

SUPPLEMENTARY MATERIAL

See the supplementary material for MoS_2 growth details, Raman spectra, atomic force microscopy (AFM) images, pump-power dependence, Decay Associated Spectra (DAS) of bare MoS_2 and VOPc samples, and table of fits for single kinetic traces and DAS.

ACKNOWLEDGMENTS

L.X.C. and M.C.S. acknowledge the partial support from CBGS, Basic Energy Science, Office of Science, the U.S. Department of Energy, through the Argonne National Laboratory under Contract No. DE-AC02-06CH11357. S.R. acknowledges his partial support from the U.S. National Science Foundation (Grant No. CHE-1955806 to L.X.C.), and C.L. acknowledges his partial support from the National Institutes of Health (under Contract No. R01-GM115761 to L.X.C.). M.P.B., V.K.S., and M.C.H. acknowledge support from the National Science Foundation Materials Research Science and Engineering Center at Northwestern University (Grant No. NSF DMR-1720139) for CVD growth and characterization of monolayer MoS_2. T.W.S. and M.C.H. acknowledge support from the National Science Foundation Division of Materials Research (Grant No. NSF DMR-2004420) for VOPc thin-film deposition and characterization. This work made use of the Keck-II facility of Northwestern University's NUANCE Center, which has received support from the SHyNE Resource (Grant No. NSF ECCS-2025633), the IIN, and Northwestern's MRSEC program (Grant No. NSF DMR-1720139). The authors acknowledge Brendan P. Kerwin for providing sublimed VOPc for quality comparison.

AUTHOR DECLARATIONS

Conflict of Interest

The authors have no conflicts to disclose.

Author Contributions

Madison C. Schwinn: Data curation (equal); Formal analysis (equal); Investigation (equal); Writing – original draft (equal); Writing – review & editing (equal). **Shahnawaz Rafiq**: Data curation (equal); Formal analysis (equal); Investigation (equal); Supervision (equal); Writing – review & editing (equal). **Changmin Lee**: Data curation (equal); Formal analysis (equal); Investigation (equal); Writing – review & editing (equal). **Matthew P. Bland**: Investigation (equal); Methodology (equal); Writing – review & editing (equal). **Thomas W. Song**: Investigation (equal); Methodology (equal); Writing – review & editing (equal). **Vinod K. Sangwan**: Investigation (equal); Methodology (equal); Writing – review & editing (equal). **Mark C. Hersam**: Conceptualization (equal); Funding acquisition (equal); Project administration (equal); Supervision (equal); Writing – review & editing (equal). **Lin X. Chen**: Conceptualization (equal); Funding acquisition (equal); Project administration (equal); Supervision (equal); Writing – review & editing (equal).

DATA AVAILABILITY

The data that support the findings of this study are available within the article and its supplementary material.

REFERENCES

[1] Z. Wang, T. Hu, R. Liang, and M. Wei, Front. Chem. **8**, 320 (2020).
[2] S. Padgaonkar, P. T. Brown, Y. Jeong, C. Cherqui, K. N. Avanaki, R. López-Arteaga, S. Irgen-Gioro, Y. Wu, V. K. Sangwan, G. C. Schatz, M. C. Hersam, and E. A. Weiss, J. Phys. Chem. C **125**, 15458–15464 (2021).
[3] A. Machín, K. Fontánez, J. C. Arango, D. Ortiz, J. De León, S. Pinilla, V. Nicolosi, F. I. Petrescu, C. Morant, and F. Márquez, Materials **14**, 2609 (2021).
[4] A. Henning, V. K. Sangwan, H. Bergeron, I. Balla, Z. Sun, M. C. Hersam, and L. J. Lauhon, ACS Appl. Mater. Interfaces **10**, 16760–16767 (2018).
[5] J. Deep, T. J. Marks, and M. Hersam, Nat. Mater. **16**, 170–181 (2017).
[6] D. Jariwala, S. L. Howell, K.-S. Chen, J. Kang, V. K. Sangwan, S. A. Filippone, R. Turrisi, T. J. Marks, L. J. Lauhon, and M. C. Hersam, Nano Lett. **16**, 497–503 (2016).
[7] D. Jariwala, V. K. Sangwan, C.-C. Wu, P. L. Prabhumirashi, M. L. Geier, T. J. Marks, L. J. Lauhon, and M. C. Hersam, Proc. Natl. Acad. Sci. U. S. A. **110**, 18076–18080 (2013).
[8] A. Gupta, T. Sakthivel, and S. Seal, Prog. Mater. Sci. **73**, 44–126 (2015).
[9] T. Kirchartz, K. Taretto, and U. Rau, J. Phys. Chem. C **113**, 17958–17966 (2009).
[10] J. W. Matthews and A. E. Blakeslee, J. Cyrst. Growth **27**, 118–125 (1974).
[11] S. Padgaonkar, J. N. Olding, L. J. Lauhon, M. C. Hersam, and E. A. Weiss, Acc. Chem. Res. **53**, 763–772 (2020).
[12] D. Kufer, I. Nikitskiy, T. Lasanta, G. Navickaite, F. H. L. Koppens, and G. Konstantatos, Adv. Mater. **27**, 176–180 (2015).
[13] P. Xia, S. Cao, B. Zhu, M. Liu, M. Shi, J. Yu, and Y. Zhang, Angew. Chem. **59**, 5218–5225 (2020).
[14] Z. Guan, Z. Xu, Q. Li, P. Wang, G. Li, and J. Yang, Appl. Catal., B **227**, 512–518 (2018).
[15] Z. Wang, L. Huang, and L. Chi, Front. Mater. **7**, 295 (2020).
[16] J.-J. Tao, J. Jiang, S.-N. Zhao, Y. Zhang, X.-X. Li, X. Fang, P. Wang, W. Hu, Y. H. Lee, H.-L. Lu, and D.-W. Zhang, ACS Nano **15**, 3241–3250 (2021).
[17] S. B. Homan, V. K. Sangwan, I. Balla, H. Bergeron, E. A. Weiss, and M. C. Hersam, Nano Lett. **17**, 164–169 (2017).
[18] A. Boulesbaa, K. Wang, M. Mahjouri-Samani, M. Tian, A. A. Puretzky, I. Ivanov, C. M. Rouleau, K. Xiao, B. G. Sumpter, and D. B. Geohegan, J. Am. Chem. Soc. **138**, 14713–14719 (2016).
[19] C. Zhong, V. K. Sangwan, C. Wang, H. Bergeron, M. C. Hersam, and E. A. Weiss, J. Phys. Chem. Lett. **9**, 2484–2491 (2018).
[20] J. Cho, N. S. Suwandaratne, S. Razek, Y.-H. Choi, L. F. J. Piper, D. F. Watson, and S. Banerjee, ACS Appl. Mater. Interfaces **12**, 43728–43740 (2020).
[21] Y. L. Huang, Y. J. Zheng, Z. Song, D. Chi, A. T. S. Wee, and S. Y. Quek, Chem. Soc. Rev. **47**, 3241–3264 (2018).
[22] Y. Kong, S. M. Obaidulla, M. R. Habib, Z. Wang, R. Wang, Y. Khan, H. Zhu, M. Xu, and D. Yang, Mater. Horiz. **9**, 1253–1263 (2022).
[23] T. Tajima, S. Okabe, and Y. Takaguchi, Bull. Chem. Soc. Jpn. **93**, 745–750 (2020).
[24] K. F. Mak, C. Lee, J. Hone, J. Shan, and T. F. Heinz, Phys. Rev. Lett. **105**, 136805 (2010).
[25] L. Yuan, T. Wang, T. Zhu, M. Zhou, and L. Huang, J. Phys. Chem. Lett. **8**, 3371–3379 (2017).
[26] V. K. Sangwan and M. C. Hersam, Annu. Rev. Phys. Chem. **69**, 299–325 (2018).
[27] R. D. Harris, S. B. Homan, M. Kodaimati, C. He, A. B. Nepomnyashchii, N. K. Swenson, S. Lian, R. Calzada, and E. A. Weiss, Chem. Rev. **116**, 12865–12919 (2016).
[28] H. Tian, M. L. Chin, S. Najmaei, Q. Guo, F. Xia, H. Wang, and M. Dubey, Nano Res. **9**, 1543–1560 (2016).
[29] S. Li, C. Zhong, A. Henning, V. K. Sangwan, Q. Zhou, X. Liu, M. S. Rahn, S. A. Wells, H. Y. Park, J. Luxa, Z. Sofer, A. Facchetti, P. Darancet, T. J. Marks, L. J. Lauhon, E. A. Weiss, and M. C. Hersam, ACS Nano **14**, 3509–3518 (2020).
[30] S. H. Amsterdam, T. K. Stanev, L. Wang, Q. Zhou, S. Irgen-Gioro, S. Padgaonkar, A. A. Murthy, V. K. Sangwan, V. P. Dravid, E. A. Weiss, P. Darancet, M. K. Y. Chan, M. C. Hersam, N. P. Stern, and T. J. Marks, J. Am. Chem. Soc. **143**, 17153–17161 (2021).
[31] X. Zhu, N. R. Monahan, Z. Gong, H. Zhu, K. W. Williams, and C. A. Nelson, J. Am. Chem. Soc. **137**, 8313–8320 (2015).
[32] X. Liu, J. Gu, K. Ding, D. Fan, X. Hu, Y.-W. Tseng, Y.-H. Lee, V. Menon, and S. R. Forrest, Nano Lett. **17**, 3176–3181 (2017).
[33] T. R. Kafle, B. Kattel, P. Yao, P. Zereshki, H. Zhao, and W.-L. Chan, J. Am. Chem. Soc. **141**, 11328–11336 (2019).
[34] X. Yu, X. Wen-Wu, and J. Zhao, J. Phys. Chem. Lett. **12**, 2312–2319 (2021).
[35] T. Zhu, L. Yuan, M. Zhao, Y. Wan, J. Mei, and L. Huang, Sci. Adv. **4**, eaao3104 (2018).
[36] N. Mutz, S. Park, T. Schultz, S. Sadofev, S. Dalgleish, L. Reissig, N. Koch, E. J. W. List-Kratochvil, and S. Blumstengel, J. Phys. Chem. C **124**, 2284–2837 (2020).
[37] S. Padgaonkar, S. H. Amsterdam, H. Bergeron, K. Su, T. J. Marks, M. C. Hersam, and E. A. Weiss, J. Phys. Chem. C **123**, 13337–13343 (2019).
[38] X.-Y. Liu, X.-Y. Xie, W.-H. Fang, and G. Cui, J. Phys. Chem. A **122**, 9587–9596 (2018).
[39] S. H. Amsterdam, T. J. Marks, and M. C. Hersam, J. Phys. Chem. Lett. **12**, 4543–4557 (2021).
[40] F. Ceballos, M. Z. Bellus, H.-Y. Chiu, and H. Zhao, ACS Nano **8**, 12717–12724 (2014).
[41] Y. L. Pan, Y. J. Wu, L. B. Chen, Y. Y. Zhao, Y. H. Shen, F. M. Li, S. Y. Shen, and D. H. Huang, Appl. Phys. A **66**, 569–573 (1998).
[42] A. Terasaki, M. Hosoda, T. Wada, H. Tada, A. Koma, A. Yamada, H. Sasabe, A. F. Garito, and T. Kobayashi, J. Phys. Chem. **96**, 10534–10542 (1992).
[43] S. Fang, H. Tada, and S. Mashiko, Appl. Phys. Lett. **69**, 767 (1996).
[44] Y. Fujikawa and S. Mashiko, Thin Solid Films **331**, 148–151 (1998).
[45] T. Niu, J. Zhang, and W. Chen, J. Phys. Chem. C **118**, 4151–4159 (2014).
[46] J. Yuan, S. E. Liu, A. Shylendra, W. A. G. Rojas, S. Guo, H. Bergeron, S. Li, H.-S. Lee, S. Nasrin, V. K. Sangwan, A. R. Trivedi, and M. C. Hersam, Nano Lett. **21**, 6432–6440 (2021).
[47] R. Aroca and R. O. Loutfy, Spectrochim. Acta, Part A **39**, 847–852 (1983).
[48] H. J. Wagner, R. O. Loutfy, and C.-K. Hsiao, J. Mater. Sci. **17**, 2781–2791 (1982).
[49] J. J. Snellenburg, S. P. Laptenok, R. Seger, K. M. Mullen, and I. H. M. van Stokkum, J. Stat. Software **49**, 1–22 (2012).
[50] K. F. Mak, K. He, J. Shan, and T. F. Heinz, Nat. Nanotechnol. **7**, 494–498 (2012).
[51] T. H. Huang and J. H. Sharp, Chem. Phys. **65**, 205–216 (1982).
[52] A. Yamashita, S. Matsumoto, S. Sakata, T. Hayashi, and H. Kanbara, Opt. Commun. **145**, 141–144 (1998).
[53] S. H. Amsterdam, T. LaMountain, T. K. Stanev, V. K. Sangwan, R. López-Arteaga, S. Padgaonkar, K. Watanabe, T. Taniguchi, E. A. Weiss, T. J. Marks, M. C. Hersam, and N. P. Stern, J. Phys. Chem. Lett. **12**, 26–31 (2021).
[54] K. M. McCreary, A. T. Hanbicki, S. V. Sivaram, and B. T. Jonker, APL Mater. **6**, 111106 (2018).
[55] T. Zheng, P. Valencia-Acuna, P. Zereshki, K. M. Beech, L. Deng, Z. Ni, and H. Zhao, ACS Appl. Mater. Interfaces **13**, 6489–6495 (2021).
[56] Y. Wang, Z. Guo, J. You, Z. Zhang, X. Zheng, and X. Cheng, Photonic Sens. **9**, 1–10 (2019).
[57] A. Splendiani, L. Sun, P. Yao, Y. Zhang, T. Li, J. Kim, C. Chim, G. Galli, and F. Wang, Nano Lett. **10**, 1271–1275 (2010).
[58] S. Das, Y. Wang, Y. Dai, *et al.* "Ultrafast transient sub-bandgap absorption of monolayer MoS_2," Light: Sci. Appl. **10**, 27 (2021).
[59] S. H. Aleithan, M. Y. Livshits, S. Khadka, J. J. Rack, M. E. Kordesch, and E. Stinaff, Phys. Rev. B **94**, 035445 (2016).
[60] W. Wang, X. Ning Sui, Z. Kang, Q. Zhou, L. H. Zhang, J. Gao, and Y. Wang, J. Phys. Chem. Lett. **12**, 861–868 (2021).
[61] E. A. A. Pogna, M. Marsili, D. De Fazio, S. Dal Conte, C. Manzoni, D. Sangalli, D. Yoon, A. Lombardo, A. C. Ferrari, A. Marini, G. Cerullo, and D. Prezzi, ACS Nano **10**, 1182–1188 (2016).
[62] D. Tsokkou, X. Yu, K. Sivula, and N. Banerji, J. Phys. Chem. C **120**, 23286–23292 (2016).
[63] I. Grigioni, L. Ganzer, F. V. A. Camargo, B. Bozzini, G. Cerullo, and E. Selli, ACS Energy Lett. **4**, 2213–2219 (2019).
[64] M. A. Khan and U. Farva, RSC Adv. **7**, 11304–11311 (2017).
[65] P. Zereshki, M. M. Tavakoli, P. Valencia-Acuna, J.-H. Park, J. Kong, and H. Zhao, Phys. Rev. B **100**, 235411 (2019).
[66] X. Xing, L. Zhao, W. Zhang, Z. Wang, H. Su, H. Chen, G. Ma, J. Dai, and W. Zhang, Nanoscale **12**, 2498–2506 (2020).
[67] H. Li, X. Zheng, Y. Liu, Z. Zhang, and T. Jiang, Nanoscale **10**, 1650–1659 (2018).